MRS Communications

Research Letter

The big bang of halide perovskites: The starting point of crystallization

Ana Palacios Saura [iD], Helmholtz-Zentrum Berlin für Materialien und Energie, Hahn-Meitner-Platz 1, 14109 Berlin, Germany; Freie Universität Berlin, Malteserstraße 74-100, 12249 Berlin, Germany

Joachim Breternitz [iD], Helmholtz-Zentrum Berlin für Materialien und Energie, Hahn-Meitner-Platz 1, 14109 Berlin, Germany; FH Münster, Stegerwaldstraße 39, 48565 Steinfurt, Germany

Armin Hoell [iD], Helmholtz-Zentrum Berlin für Materialien und Energie, Hahn-Meitner-Platz 1, 14109 Berlin, Germany

Susan Schorr [iD], Helmholtz-Zentrum Berlin für Materialien und Energie, Hahn-Meitner-Platz 1, 14109 Berlin, Germany; Freie Universität Berlin, Malteserstraße 74-100, 12249 Berlin, Germany

Address all correspondence to Ana Palacios Saura at **ana.palacios_saura@helmholtz-berlin.de**

Abstract

Hybrid halide perovskites (HHPs) are very promising absorber materials for solar cells due to their high power conversion efficiency and the low-cost solution-based processing methods. We applied small angle X-ray scattering to $MAPbI_3$, $FAPbI_3$ and $MAPbBr_3$ precursor solutions in different solvents (GBL, DMF, and mixtures) to gain a deeper understanding of the building blocks during the early stage of HHP formation. We present a core–shell model where the core is formed by $[PbX_6]$ octahedra surrounded by a shell of solvent molecules, which explains the arrangement of the precursors in solution and how the solvent and the halide influence such arrangement.

Introduction

Hybrid halide perovskites (HHPs) have become extremely popular for a number of applications, such as LEDs,[1] photodetectors,[2] and most importantly, for photovoltaics.[3] Due to their outstanding properties as absorber materials for solar cells, they are particularly of interest among the photovoltaic community since the power conversion efficiency (PCE) of perovskite-based solar cells has sky-rocketed reaching up to 26.1% in 2023.[4]

HHPs have an ABX_3 composition and crystallize in the perovskite-type structure. Here, A is a monovalent organic cation, typically methylammonium (MA^+) or formamidinium (FA^+), B is a divalent metallic cation such as Pb^{2+} or Sn^{2+}, and X is a halide, I^-, Br^-, or Cl^-. The bandgap energy of HHPs can be tuned when varying their composition by exchanging the anion or the cations[5] making this material ideal for single junction as well as for tandem solar cell applications. As an example, the bandgap energy of $MAPb(I_{1-x}Br_x)_3$ can be tuned continuously from 1.56 to 2.3 eV.[6] HHPs can be synthesized from solution at low temperatures.[7–10] It has been shown that the choice of the solvent not only affects the crystallization path of HHPs,[11,12] but also the power conversion efficiency of the solar cell.[13] Therefore, understanding the formation mechanism of HHPs in the solution is a key point for controlling the crystallization process and ultimately improving the performance of a device produced from solution processing. It has been reported in literature the existence of highly valent iodoplumbates in HHPs precursor solution[14] as well as the possibility of achieving a power conversion efficiency of 20% using solvent engineering[15] showing how important it is to understand the solvation chemistry in HHPs precursor solutions.

Flatken et al.[16] demonstrated that small angle X-ray scattering (SAXS) is a powerful technique to investigate HHPs precursor solutions in the nanometer range. They showed the existence of colloidal nanostructures in $MAPbI_3$ precursor solutions using a mixture of dimethylformamide (DMF) and dimethyl sulfoxide (DMSO) as solvent in a range of concentrations, from 0.4 M to 1.2 M. With this study, we aim to bring more clarity about the precursor arrangement in solution prior to crystallization and how the solvent affects the atomic arrangement in this early state. We applied SAXS to investigate the precursor solutions of $MAPbI_3$, $FAPbI_3$, and $MAPbBr_3$ in different common solvents used to synthesize HHPs layers, such as γ-butyrolactone (GBL), dimethylformamide (DMF), and mixtures thereof while keeping the concentration constant to 0.8 M. In this first approach to understand the role of the solvent in the early-stage crystallization of HHPs, we chose GBL and DMF as solvents since they are frequently used to synthesize HHP single crystal, bulk as well as thin films. The Gutmann's donor number (DN) is a parameter used to predict how a solvent is able to solvate HHP precursors,[17] increasing DN indicates that the solvent is more likely to coordinate with Pb^{2+}, competing with I^-. On the other hand, a lower DN favors the formation of iodoplumbates since it is less likely to coordinate with Pb^{2+}. Since GBL has a lower DN than DMF (18 and 26.6[18] kcal/mol, respectively), it is expected that the iodoplumbates in solution when GBL is used as solvent are larger than the iodoplumbates present in the solution when DMF is used as solvent. SAXS is a non-destructive characterization technique based on the scattering length density difference between the scattering objects and the matrix. SAXS allows us to determine the average distance between the centers of mass of adjacent scattering objects as

well as the form factor and the structure factor. The form factor contains information about the size and shape of the nanoparticles (scattering objects), whereas the structure factor describes the interaction between them.[19–21] Herein, we conclude that the choice of solvent and the anion affect the arrangement of the precursors in HHPs solutions and therefore have the potential to influence the crystallization path.

Experimental
Synthesis
$MAPbI_3$, $FAPbI_3$, and $MAPbBr_3$ precursor solutions were synthesized using a method adapted from Im et al.[22] All the chemicals were used as received without further purification. The halide perovskite precursor solutions were prepared mixing 0.8 M of PbI_2 (Tokyo Chemical Industry, >98%) and MAI (CH_3NH_3I), FAI ($CH(NH_2)_2I$), or MABr (CH_3NH_3Br) (Tokyo Chemical Industry, >99%), respectively, in a solvent (GBL, DMF, Tokyo Chemical Industry, >99%). $MAPbI_3$ precursor solutions were prepared mixing stoichiometric amounts of MAI and PbI_2 using the following GBL:DMF solvent ratios: 100% GBL, 90:10, 80:20, 70:30, 60:40, 50:50, 40:60, 30:70, 20:80, 10:90, and 100% DMF. $FAPbI_3$ precursor solutions were prepared mixing stoichiometric amounts of FAI and PbI_2 using the following GBL:DMF solvent ratios: 100% GBL, 50:50, and 100% DMF. $MAPbBr_3$ precursor solution was processed mixing stoichiometric amounts of MABr and $PbBr_2$ using 100% DMF as solvent. The solutions were stirred at 60 °C for 60 min under nitrogen atmosphere. Afterward, the precursor solutions were transferred into a thin (wall thickness of 0.1 mm) rectangular borosilicate capillary purchased from CM Scientific, UK.

Density functional theory (DFT) modeling
The bond length between the Pb^{2+} ion and the halogen (X^-) was calculated by optimizing the structure of $[PbX_6]^{4-}$ octahedra using Hartree–Fock (HF) calculations with nwchem7.0.2[23] and the UGBS basis set.[24] The outer radius of X^- was defined as 95% probability of the integrated electron density (Table I).

The structures of GBL and DMF were modeled using an optimized model made with HF [23] with a 6-31g basis set. Further, Slater radii were added to the atoms in order to model their size.[25] The overall shape of the molecules was then described by calculating minimal volume enclosing ellipsoids using the mvee method of the qinfer library in python3. The resulting ellipsoid is described by 3 radii (r_{s1}, r_{s2} and r_{s3}) (Table II).

Table I. Bond lengths between lead and the halide and halide radii calculated with DFT.

Bond	Bond length (nm)	Anion X^-	Radius anion r_{X^-} (nm)
Pb − I	0.319	I^-	0.165
Pb − Br	0.288	Br^-	0.137

Characterization
Synchrotron small angle X-ray scattering (SAXS)
All the precursor solutions were measured at the HZB's synchrotron radiation source BESSY II, at the four-crystal monochromator beamline[26] in the laboratory of the Physikalisch-Technische Bundesanstalt using the Helmholtz-Zentrum Berlin (HZB) ASAXS instrument[27] at room temperature. The SAXS patterns were recorded using a windowless DECTRIS 1M PILATUS2 in vacuum hybrid pixel detector. The measurements were carried out at 10 keV with a distance between the sample and the detector of 0.8 m, therefore, a q-range from 0.2 to 8 nm^{-1} (size range: 31.41–0.79 nm) was covered. Each sample was measured twice at three different points along the capillary for 3 min, being the total exposure 18 min/sample. The 2D scattering images were azimuthally averaged to 1D scattering curves around the beam center. The data were analyzed using the software SASfit.[28]

Results and discussion
The SAXS pattern obtained from the measurements of $MAPbI_3$, $FAPbI_3$, and $MAPbBr_3$ precursor solutions show a clear maximum in the scattered intensity at q-values of approximately 2.5–3.7 nm^{-1} [Figure 1(a)]. The average distance between scattering objects (d_{exp}) can be calculated using the peak position (q_{max}) applying Eq. 1 [Figure 1(b)]. The peak position was determined by a single peak fit using the PseudoVoigt1 function.

$$d_{exp} = \frac{2\pi}{q_{max}}, \qquad (1)$$

There is a clear correlation between the fractions of GBL and DMF in the solvent and the average distance between the scattering objects, d_{exp}. In both $MAPbI_3$ and $FAPbI_3$ precursor solutions, d_{exp} increases with increasing GBL content in the GBL:DMF solvents. This trend indicates that the scattering objects formed in higher GBL content are larger than those formed with higher DMF content. Moreover, exchanging the halide from iodide to bromide decreases d_{exp} even further. On the other hand, exchanging MA^+ for FA^+ as the A-cation does not have a significant impact on d_{exp}. The distance between scattering objects in $MAPbI_3$ precursor solution ranges from 1.956±0.020 in DMF to 2.306±0.020 nm in GBL, in case of $FAPbI_3$ precursor solution, d_{exp} is in the range of 1.949±0.020 nm in DMF to 2.271±0.020 in GBL and the d_{exp} in $MAPbBr_3$

Table II. Radii of GBL and DMF calculated with DFT.

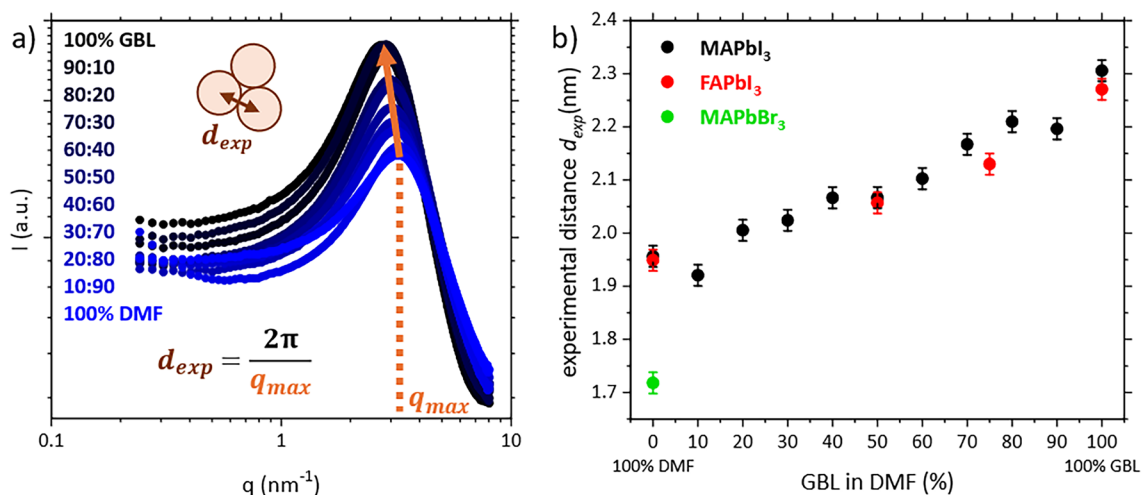| Solvent	r_{s1} (nm)	r_{s2} (nm)	r_{s3} (nm)
GBL	0.188	0.211	0.314
DMF	0.150	0.245	0.306

Figure 1. (a) SAXS patterns of MAPbI$_3$ in a range of GBL:DMF mixtures. The peak shifts toward lower q-values with increasing GBL content. (b) Distance between scattering objects in solution for MAPbI$_3$, FAPbI$_3$, and MAPbBr$_3$ precursor solutions. Increasing the amount of GBL in the solvent ratio increases the distance between scattering objects linearly for both MAPbI$_3$ and FAPbI$_3$.

precursor solution in DMF is 1.718 ± 0.020 nm. The difference in the distance between the scattering objects in DMF and GBL cannot be explained solely by the size difference between the solvent molecules.

While all solutions show agglomerations, we are able to demonstrate that the size of those agglomerates changes not only with the composition of HHP precursors, but also with the solvent. Based on this information, we have developed a core–shell model to describe the scattering objects, with [PbX$_6$] (X=I$^-$, Br$^-$) octahedra in the core surrounded by solvent molecules [Figure 2(a)]. Based on this information, we have developed a core–shell model to describe the scattering objects, with [PbX$_6$] (X=I$^-$, Br$^-$) octahedra in the core surrounded by solvent molecules [Figure 2(a)]. This model combines the information obtained by SAXS using different solvents as well as the information from Radicchi et al.

and Flatken et al.[14,16] where they indicate the presence of highly valent iodoplumbates in solution. For this model, we considered three assumptions: firstly, the scattering objects agglomerate, as shown by the structure factor; we consider that they are spherical, as shown by the form factor; and lastly, we do not consider the interaction between the solvent and Pb^{2+}. The [PbX$_6$] octahedra in the core can be arranged as a single octahedron [PbX$_6$]$^{4-}$ or as corner-sharing octahedra [Pb$_2$X$_{11}$]$^{7-}$. When the core is formed by a single octahedron, the radius of the core (r_{core}) can be described as the sum of the Pb-X bond length and the radius of the outer anion (r_{X^-}) (Eq. 2). Whereas, when the core is composed of a corner-sharing octahedra, its radius is calculated as the sum of twice the Pb-X bond length and the radius of the outer anion (Eq. 3).

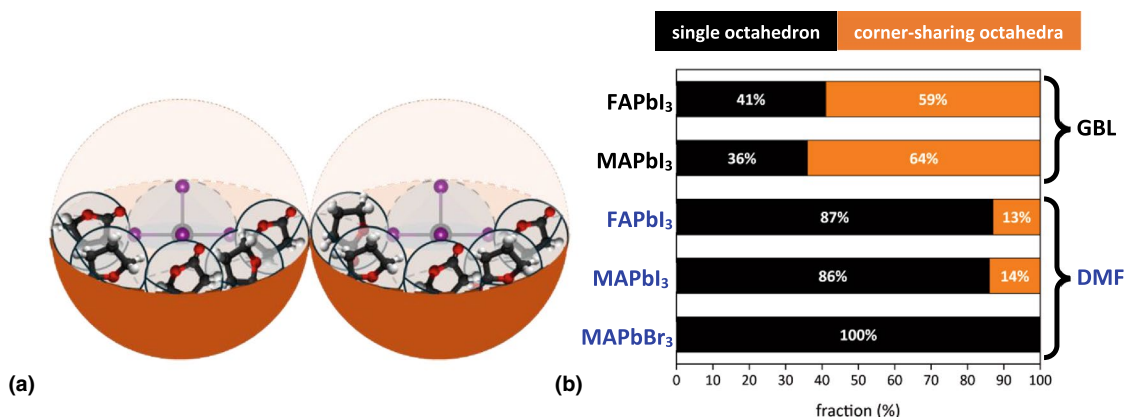$$r_{core}^{single\,octahedra} = Pb - X + r_{X^-}, \qquad (2)$$

Figure 2. (a) Core–shell model of two adjacent scattering objects with a single [PbX$_6$] octahedra in the core and randomly oriented GBL solvent molecules as the shell. (b) Proportion of single octahedra (black) and corner-sharing octahedra (orange) in the core. The use of DMF as solvent and bromide as halogen favor the single octahedra arrangement in the core of the scattering objects.

$$r_{core}^{corner-sharing} = 2 \cdot (Pb - X) + r_{X^-}. \qquad (3)$$

The core is surrounded by a shell of solvent molecules which were modeled as ellipsoids (Table II). We considered the ellipsoids to be randomly oriented, therefore the geometric mean ($\bar{r}_s$) (Eq. 4) of the ellipsoid radii was used to calculate the radius of the solvent.

$$\bar{r}_s = \sqrt[3]{r_{s1} r_{s2} r_{s3}}. \qquad (4)$$

Combining the two core arrangements and the radius of the solvent, we can describe the distance between two adjacent scattering objects as Eq. 5:

$$d_{model} = 2r_{core} + 4\bar{r}_s. \qquad (5)$$

As a result, we can explain the average distance between the scattering objects, d_{exp}, obtained from the peak position in the SAXS pattern applying the core–shell model with a combination of single octahedra and corner-sharing octahedra [PbX$_6$] arrangement in the core and surrounded by randomly oriented solvent molecules. We found that the solvent has a major influence on how the [PbX$_6$] octahedra in the core are arranged. Most of the cores in the precursor solutions prepared with GBL are arranged as corner-sharing octahedra for both MAPbI$_3$ and FAPbI$_3$; however, when DMF is used as solvent instead, most of the cores are arranged as single octahedra [Figure 2(b)]. Moreover, in case of MAPbBr$_3$ precursor solution, we found that all the cores in the scattering objects are arranged as single octahedra. This shows that although the effect of the solvent is stronger than the halide, the effect of the halide in the precursors arrangement of HHPs cannot be neglected.

The structural information was obtained by fitting the SAXS patterns using SASfit,[28] the data were fitted to a model-based form factor. We modeled the shape of the scattering objects as spheres for all the studied precursor solutions. The analysis of the SAXS data performed with SASfit showed that MAPbI$_3$ and FAPbI$_3$ precursor solutions are formed by polydisperse scattering objects, which follow a lognormal size distribution. The median of both size distributions was fixed to 0.319 nm, which is Pb–I bond length. The polydispersity of the scattering objects increases with increasing GBL content, indicating that the precursor solution become more heterogeneous. Furthermore, MAPbBr$_3$ precursor solution is composed of monodisperse scattering objects. The radius of the MAPbBr$_3$ monodisperse particles is 0.259 ± 0.001 nm. These results are in agreement with the proposed core–shell model.

The interaction between the scattering objects (structure factor) was modeled as a hard sphere following the monodisperse Percus–Yevick approximation.[29,30] The hard sphere model is based on the assumption that the scattering objects cannot be compressed and they cannot penetrate each other. The structure factor can be described as a function of the radius of the hard sphere (R_{HS}) and the volume fraction of the spheres (f_p), being R_{HS} the minimum possible distance between the scattering objects and f_p the measure of

interacting scattering objects in the solution. We found that the R_{HS} is smaller than half of the average distance between scattering objects, d_{exp}, which is the radius of one scattering object (core being a mixture of single and corner-sharing octahedra surrounded by randomly oriented solvent molecules). This phenomenon indicates that the scattering objects must be able to achieve a more compact arrangement. The minimum distance between the scattering objects can be explained by having only single octahedra in the core surrounded by oriented solvent molecules in the shell (Eq. 6):

$$R_{HS} = r_{core}^{singleoctahedra} + 2r_s^{app}, \qquad (6)$$

where R_{HS} is the radius of the hard sphere, $r_{core}^{singleoctahedra}$ is the radius of the core when it is arranged as a single octahedron, and r_s^{app} is the radius of the solvent when the ellipsoid used to describe the solvent molecule is oriented.

Conclusion

In this study, we demonstrate that the choice of solvent for solution-based hybrid halide perovskites has a strong influence on the atomic arrangement of the precursors. We show that increasing the amount of GBL in a GBL:DMF precursor solution also increases the distance between the scattering objects in MAPbI$_3$ and FAPbI$_3$ solutions. We developed a core–shell model to describe the average distance between scattering objects d_{exp}, where the core is formed by PbX$_6$ octahedra arranged as single octahedra or corner-sharing octahedra and the shell is composed of randomly oriented solvent molecules surrounding the core. The ratio between single octahedra and corner-sharing octahedra varies with the GBL:DMF ratio. Increasing DMF content in the solution also increases the amount of single octahedra in both FAPbI$_3$ and MAPbI$_3$ precursor solutions. In case of MAPbBr$_3$ precursor solution, we show that the core of the scattering objects is formed by single octahedra only. This is in agreement with the result that in this case the precursor solution is composed of monodisperse scattering objects. Moreover, we found that Br$^-$ as halogen also favors the formation of single octahedra in the core although the effect of the solvent is stronger. We also demonstrate that the A-cation does not influence the core atomic arrangement. The scattering objects in the solutions were modeled as spheres. The SAXS analysis showed that MAPbBr$_3$ precursor solution is formed by monodisperse spheres, whereas MAPbI$_3$ and FAPbI$_3$ precursor solutions are formed by polydisperse spheres described by a lognormal size distribution. The conclusions derived from the structural information, obtained by fitting the SAXS patterns using SASfit, are in agreement with the proposed core–shell model. This study was focused on MAPbI$_3$, FAPbI$_3$ and MAPbBr$_3$ precursor solutions; however, it can be expanded to other compositions or other solvents. We investigated the role of the A-cation in the core–shell model by probing compositions with inorganic A-cations [A. Palacios Saura et al., in preparation], as well as the effects of other solvent, such as NMP and DMSO [A. Palacios Saura

et al., in preparation]. These results will be published in following papers. Since perovskite-based solar cells are mostly produced from solution, it is crucial to understand how HHPs are formed. As Huang et al.[13] showed, the choice of solvent can ultimately impact the efficiency of a perovskite-based solar cell. This study gives an insight on how the precursors are arranged in solution, showing that the solvent is not only the media for the reaction, but participates in the crystallization process. This research contributes to a better understanding of the formation mechanism of hybrid halide perovskites, which can be used for any solution-processed HHP-based solar cell device as well as any other applications by solvent engineering, in this way having an impact on the materials community.

Author contributions

All authors contributed equally to this work.

Data availability

The associated data are provided in the supplementary information.

Declarations

Conflict of interest

On behalf of all authors, the corresponding author states that there is no conflict of interest.

Supplementary Information

The online version contains supplementary material available at https://doi.org/10.1557/s43579-024-00611-x.

Open Access

References

1. A. Fakharuddin, M.K. Gangishetty, M. Abdi-Jalebi, S.-H. Chin, A.R. bin Mohd Yusoff, D.N. Congreve, W. Tress, F. Deschler, M. Vasilopoulou, H.J. Bolink, Nat. Electron. **5**, 203–216 (2022). https://doi.org/10.1038/s41928-022-00745-7
2. C. Bao, J. Yang, S. Bai, W. Xu, Z. Yan, Q. Xu, J. Liu, W. Zhang, F. Gao, Adv. Mater. **30**, 1803422 (2018). https://doi.org/10.1002/adma.201803422
3. A.D. Shpatz, S. Rahmany, M. Flatken, T. Binyamin, A. Hoell, A. Abate, L. Etgar, Mater. Adv. **3**, 1737–1746 (2022). https://doi.org/10.1002/adma.201803422
4. NREL: Best Research-Cell Efficiency Chart. https://www.nrel.gov/pv/cell-efficiency.html
5. S.A. Kulkarni, T. Baikie, P. Boix, N. Yantara, N. Mathews, S. Mhaisalkarab, J. Mater. Chem. A **2**, 9221 (2014). https://doi.org/10.1039/c4ta00435c
6. J.H. Noh, S.H. Im, J.H. Heo, T.N. Mandal, S. Il Seok, Nano Lett. **13**, 1764–1769 (2013). https://doi.org/10.1021/nl400349b
7. M.I. Saidaminov, A.L. Abdelhady, B. Murali, E. Alarousu, V.M. Burlakov, W. Peng, I. Dursun, L. Wang, Y. He, G. Maculan, A. Goriely, T. Wu, O.F. Mohammed, O.M. Bakr, Nat. Commun. **6**, 1–6 (2015). https://doi.org/10.1038/ncomms8586
8. Y. Rakita, O. Bar-Elli, E. Meirzadeh, H. Kaslasi, Y. Peleg, G. Hodes, I. Luborirsky, D. Oron, D. Ehre, D. Cahen, Proc. Natl. Acad. Sci. U.S.A. **114**, E5504–E5512 (2017). https://doi.org/10.1038/ncomms8586
9. Y. Dang, Y. Liu, Y. Sun, D. Yuan, X. Liu, W. Lu, G. Liu, H. Xia, X. Tao, Cryst. Eng. Comm. **17**, 665–670 (2015). https://doi.org/10.1039/c4ce02106a
10. H.-S. Kim, C.-R. Lee, J.-H. Im, K.-B. Lee, T. Moehl, A. Marchioro, S.-J. Moon, R. Humphry-Baker, J.-H. Yum, J.E. Moser, M. Grätzel, N.-G. Park et al., Sci. Rep. **2**, 591 (2012). https://doi.org/10.1038/srep00591
11. S.A. Fateev, A.A. Petrov, V.N. Khrustalev, P.V. Dorovatovskii, Y.V. Zubavichus, E.A. Goodilin, A.B. Tarasov, Chem. Mater. **30**, 5237–5244 (2018). https://doi.org/10.1021/acs.chemmater.8b01906
12. A. Petrov, S.A. Fateev, V.N. Khrustalev, Y. Li, P.V. Dorovatovskii, Y.V. Zubavichus, E.A. Goodilin, A.B. Tarasov, Chem. Mater. **32**, 7739–7745 (2020). https://doi.org/10.1021/acs.chemmater.0c02156
13. P.-H. Huang, Y.-H. Wang, J.-C. Ke, C.-H. Huang, Energies **10**, 599 (2017). https://doi.org/10.1021/acs.chemmater.0c02156
14. E. Radicchi, E. Mosconi, F. Elisei, F. Nunzi, F. De Angelis, A.C.S. Appl, Energy Mater. **2**, 3400–3409 (2019) https://doi.org/10.1021/acsaem.9b00206
15. T. Wu, J. Wu, Y. Tu, X. He, Z. Lan, M. Huang, J. Lin, J. Power Sources **365**, 1–6 (2017). https://doi.org/10.1016/j.jpowsour.2017.08.074
16. M.A. Flatken, A. Hoell, R. Wendt, E. Härk, A. Dallmann, A. Prause, J. Pascual, E. Unger, A. Abate, J. Mater. Chem. A **9**, 13477–13484 (2021). https://doi.org/10.1039/D1TA01468D
17. V. Guttmann, Electrochim. Acta **21**, 661–670 (1976). https://doi.org/10.1016/0013-4686(76)85034-7
18. F. Cataldo, Eur. Chem. Bull. **4**, 92–97 (2015)
19. O. Glatter and O. Kratky, Academic Press (1982)
20. L. A. Feigin and D. I. Svergun, Springer, vol. 1 (1987)
21. H. Schnablegger and Y. Singh, Anton Paar GmbH (2013)
22. J.-H. Im, C.-R. Lee, J.-W. Lee, S.-W. Park, N.-G. Park, Nanoscale **3**, 4088–4093 (2011). https://doi.org/10.1039/c1nr10867k
23. E. Aprà, E.J. Bylaska, W.A. de Jong, N. Govind, K. Kowalski, T.P. Straatsma, M. Valiev, H.J.J. van Dam, Y. Alexeev, J. Anchell, V. Anisimov, F.W. Aquino, R. Atta-Fynn, J. Autschbach, N.P. Bauman, J.C. Becca, D.E. Bernholdt, K. Bhaskaran-Nair et al., J. Chem. Phys. **152**, 184102 (2020). https://doi.org/10.1063/5.0004997

24. E.V.R. de Castro, F.E. Jorge, J. Chem. Phys. **108**, 5225–5229 (1998). https://doi.org/10.1063/1.475959
25. J. Slater, Chem. Phys. **41**, 3199–3204 (1964). https://doi.org/10.1063/1.1725697
26. M. Krumrey, G. Ulm, Nucl. Instrum. Methods Phys. Res. Sect. A **467–468**, 1175–1178 (2001). https://doi.org/10.1016/S0168-9002(01)00598-8
27. A. Hoell, I. Zizak, H. Bieder and L. Mokrani, DE102006029449 (2007)
28. I. Breßler, J. Kohlbrecher, A.F. Thünemann, J. Appl. Cryst. **48**, 1587–1598 (2015). https://doi.org/10.1107/S1600576715016544
29. J.K. Percus, G.J. Yevick, Phys. Rev. **110**, 1–13 (1958). https://doi.org/10.1103/PhysRev.110.1
30. A. Vrij, J. Chem. Phys. **3267**, 3267–3270 (1979). https://doi.org/10.1063/1.438756